Experimental Examination of the Liquid Sheet Disintegration Process Using Combined Photography and Fiber Based Measuring Techniques

E. Musemic*, M. Gaspar†, F. Weichert†, H. Müller† and P. Walzel*
* Department of Biochemical Engineering
† Department of Computer Science
Dortmund University of Technology
Dortmund, D-44227 Germany

Abstract

The behavior of liquid sheets in ambient air is examined with a combination of conventional photography methods and a fibre based sensor technique. This combination allows a detailed insight into the sheet flow behavior ahead of the drop formation process, such as sheet velocity, oscillation frequency and amplitude, spray angle and sheet break-up length. The proximate evaluation of the raw image data was performed using contour tracking and image filtering techniques, enabling a fully automated evaluation of whole data sets. The investigation has shown an interrelation between the sheet frequencies and the growth of aerodynamic waves, as well as the spray angles and break-up lengths depending on the operating conditions, liquid properties and nozzle geometry. Within the range examined, the frequency analysis of the sheet oscillation shows dominating oscillation frequencies at all flow conditions. With growing distance to the nozzle orifice, the dominating frequency remains constant. The decrease in sheet thickness due to its spread along divergent streamlines, as well as caused by the growth of wave amplitudes can also be measured indirectly.

Introduction

Pressure-swirl atomizers are found in a wide range of technical applications, such as injection of fuels into combustion chambers, spray drying for granules production, waste gas cleaning in scrubbing towers and many others. In general, well defined i.e. narrow drop size distributions and small drop-to-nozzle diameter ratios are desired. Since the disintegration process of the liquid sheet is of significant importance for the resulting drop sizes, the knowledge of the transition from a continuous sheet to single drops is of practical interest. An experimental reliable evidence of conformity to the different theoretical approaches could not yet be presented so far, not at least because of the highly demanding task of the experimental analysis. Liquid atomization processes seem to be too complex to allow a purely theoretical study. Therefore experimental studies are necessary to verify and improve the existing theoretical models, by means of a quantification of relevant sheet characteristics.

Inside a pressure-swirl nozzle, a swirl-flow of the liquid is induced by one or multiple tangential oriented liquid inlets, which lead to a positive pressure gradient in radial direction. At a certain radius, the local liquid pressure falls below the pressure of the ambient gas, leading to an internal air core along the pivot axis of the nozzle. In this manner, the air-core is blocking a part of the nozzle outlet, while the liquid emerges along straight trajectories in a shape of a hyperbolic sheet. During the film propagation, Kelvin-Helmholtz type of instability arises, leading to growth of initial sheet displacements along the streamlines due to the aero-dynamical stimulation in the ambient gas. In this way, the sheet oscillation is amplified and finally causes the sheet to break into fragments, which is often classified as the primary break-up process [1]. The rim contraction of broken sheet fragments leads to ligaments, which later on resolve to single droplets. This secondary break-up process is initiated by the Rayleigh type instability. In general, the first stage of the break-up process is described via classical linear stability theories, as shown in [2] and [3], while drop sizes correspond mostly to existing theories based on mass balances and contraction of the sheet fragments. Newer theoretical approaches, as described in [4], [5] and [6] consider three-dimensional effects, such as the presence of lateral waves, which are found to have a considerable influence on the sheet disintegration process.

While the flow rates at given pressures are easily accessible, the determination of the spray cone angles, the sheet break-up lengths and the oscillation characteristics is more challenging. The measurement of spray angles as well as the localization of the sheet break-up position can be performed with photographical methods, as shown in [7]. The determination of sheet velocities by means of particle image velocimetry (PIV) is also proposed, but instead of using particles, the sheet texture is used to track the sheet movement. Due to the higher spatial and temporal resolution and their ability to determine sheet velocity and oscillation frequencies at the

* Corresponding author: emir.musemic@bci.tu-dortmund.de

same time, fiber-optical sensors [8] may be used to supplement the photographical approach, allowing for a more complete view on the mechanisms during the primary drop formation process.

Experimental Setup

The experimental setup consists of the atomization plant with variable nozzle geometries and two measuring systems, i.e. the photographical setup and the fiber-optical sensor. The atomization plant allows operating at different pressures and temperatures, as well as the possibility of mounting different nozzles. In general, the nozzle has two tangential fluid inlets, each with an inner diameter D_E, into the swirl chamber, as shown in Figure 1. The swirl chamber bottom is cone-shaped, restricting the swirl chamber diameter D_K toward the nozzle orifice. The orifice may include a cylindrical part with a L/D-ratio of 1, while a L/D-ratio of 0 means a sharp edged nozzle orifice. The nozzle material is PVC, with practically smooth surface. The experimental fluid is collected in an open reservoir and conveyed to the nozzle with a rotary pump in a recycle loop, where the liquid temperature was controlled using a cooling/heating coil.

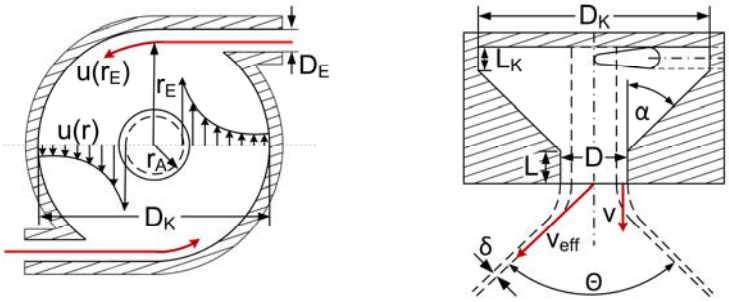

Figure 1 Dimensional sketch of the nozzle design

The different nozzle geometries are realized by fitting different nozzle parts from a kit, so that the size of inlet ports dimensions of the swirl chamber and outlet geometry could be changed independently. An overview of the evaluated nozzle geometries is listed in Tab. 1. Here, the ratio between the tangential and the axial velocity component, as shown in Fig. 1, may be described by introducing the dimensionless swirl-ratio Δ , which consists of geometrical values only. The higher the swirl-ratio Δ, the higher the tangential velocity component u and the higher the expected spray angle produced by the nozzle.

$$\Delta = \frac{\pi\, r_E\, D}{4\, A_E} = \frac{D\left(D_K - D_E\right)}{2\, D_E} \sim \frac{u}{v} \tag{1}$$

Table 1 Geometrical data of the examined nozzles

	D	D_K	D_E	L/D	Δ		D	D_K	D_E	L/D	Δ
Nozzle 1	8	35	7	0	2.29	Nozzle 5	12	50	7	1	5.27
Nozzle 2	8	35	7	1	2.29	Nozzle 6	15	50	7	0	6.58
Nozzle 3	8	50	7	0	3.51	Nozzle 7	15	50	7	1	6.58
Nozzle 4	12	50	7	0	5.27	Nozzle 8	15	50	9	0	3.80

The photographical setup is based on the backlighting principle, where the light source is oriented opposite to the camera position, allowing for low exposure time while keeping the overall image brightness high. The image object is located between the camera and the light source. In this context, it is important to achieve low exposure times in order to keep the in-motion unsharpness of the image object low, since the sheet velocity is expected to be in the range between 5 an 20 m/s, depending on the atomization pressure. As the illuminated area is 150 x 150 mm wide, the main problem is to maintain a uniform spatial light intensity. For this purpose, a LED based light source was developed. 1800 super-bright red LEDs, each with a diameter of 10 mm, were soldered on a circuit board. The dimensions of this circuit board are 400 x 500 mm, which also defines the illumination area. The LEDs have an illumination angle of 30 deg and allow the placement of the panel far behind the focal plane. Thus, the single LEDs appear blurred, forming a clear white image background. An electronic circuit generates pulses with pulse duration of 10 µs when triggered externaly. Because of the short pulse duration, the LEDs can stand a massive overcurrent, thus leading to high illumination intensity. In opposite of the LED-panel, a PCO Pixelfly CCD-camera (1280x1024 pixel, 8-bit greyscale) is assembled. The focal plane of the object lens

was adjusted in such way, that the outside boarders of the sheet defining the spray angle, are captured with high sharpness.

The second measuring system used in the present work is the fiber-optical sensor, which was already presented in past investigations [6][8]. Therefore, only a brief description of the measuring principle is given in the following. The measuring technique exploits the Fresnel effect on the plane fiber end to detect differences in the refractive index between fiber and the fluid at the fiber tips. The intensity of the reflected light can be measured with a photo diode on the remote tip of the fiber, as the fiber is transmitter and receiver at the same time. Assembling multiple fibers in a row, local changes in the refractive index can be detected along a line. In the present case, such differences are caused by the phase-change on the fibre tips, when the fiber is positioned inside of the oscillating sheet. The fiber-array is oriented perpendicular to the sheet surface, allowing the detection of local sheet displacements over time.

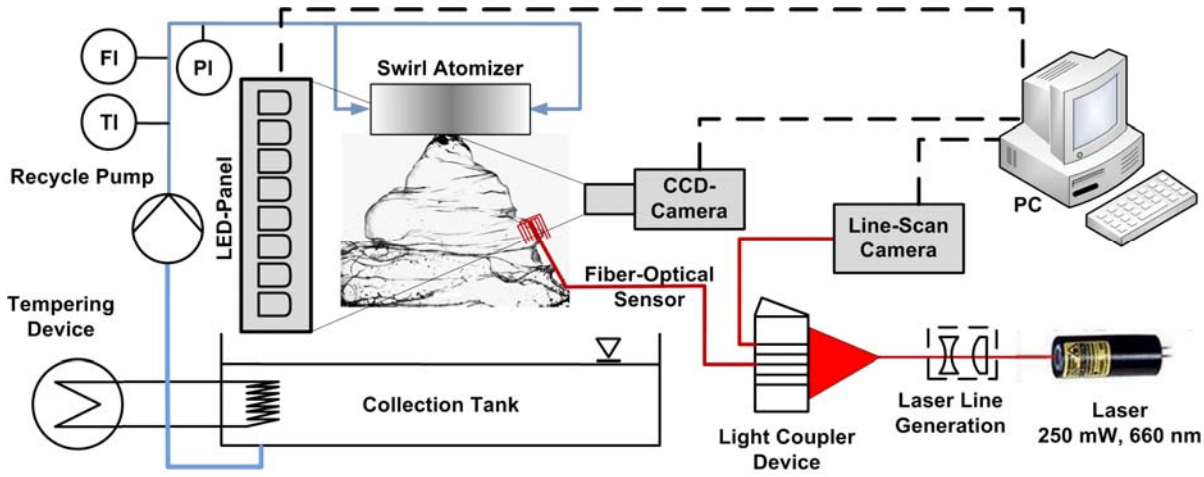

Figure 2 Experimental setup with combined fiber-optical and photographical measuring devices

In this work, two fiber-arrays were bundled to a double sensor, allowing also the measurement of sheet velocity. Each fiber array consists of 110 multi-mode PMMA fibers with an outer diameter of 250 micron and a numerical aperture of 0.5. In the past, more than two sensors were used in order to obtain frequencies in lateral direction [6]. The main advantage of the fiber-sensor over conventional PIV is its higher temporal and spatial resolution. On the other hand, its invasive nature may influence the drop formation process. However, the influence was proven with conventional high speed imaging and is found to be negligible, as long as the fiber dimensions are in the same order of magnitude as the sheet thickness.

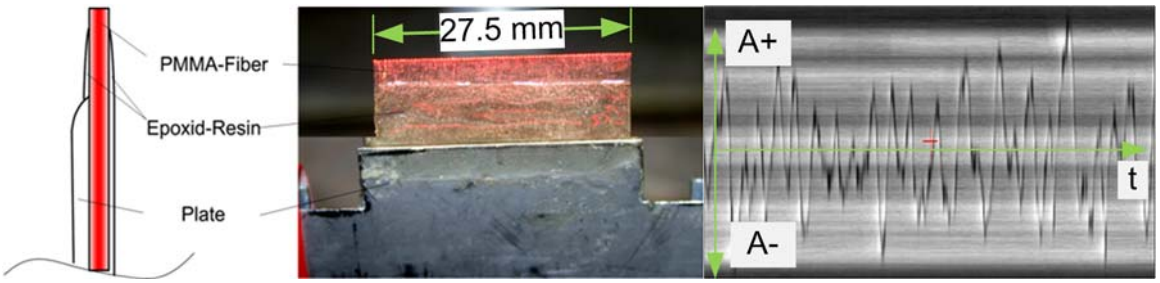

Figure 3 left: fiber-sensor assembling, right: raw signal of the local sheet displacement over time

The distance between the sensors and the nozzle orifice was graduated in steps of 5 mm, which allows for taking readings along the moving path of the sheet. The light source of the measuring system is a 300 mW laser diode, with a wavelength of 660 nm. The light is focused and coupled into the fibers by using a bending coupler device [9][10], which consists of a metal wedge with an angle of 30 deg. The lamella signal is being recorded by a line-scan CCD camera directly mounted at the remote tip of the fibers. Thus, the fibers in this setup are acting as signal transmitters and receivers at the same time. The camera model is a DALSA Piranha 3 line scan camera with a maximum sampling rate of 33.7 kHz. With this setup, the motion of the oscillating sheet impinging on the sensor is recorded with a maximum spatial resolution of 250 µm and 30 µs in time. Every image consists of 10000 lines, recorded with a sampling rate of 33.7 kHz, which is equivalent to an observed time period of 0.297 s for each image. For every setting 10 images were recorded and analysed. The high time resolution of the measuring system permits accurate measurement of sheet displacements at every single position along the main streamline of the moving sheet, except positions very close to the nozzle due to the sensor dimensions. Using

water-glycerol mixtures, the viscosity range between 1 and 50 mPas was covered. The atomization pressure was graduated in steps between $0.3 < \Delta p < 2.0$ bar.

Data Evaluation

The procedure of extracting a discrete function representing the lamella from a photo is visualized in Fig. 3. The nozzle in the top region of the images has known dimensions and is a constant and irrelevant feature in all images. This leads to template based approach to remove the nozzle and thereby isolate the interesting region of the image from the top. Just below the nozzle, there are varying sheet structures, which are found to be easily accessible due to the homogeneous light source in the background. For a rough separation of the sheet structures from the background in that region, a fuzzy-clustering based thresholding turned out to be sufficient [11]. The lamella itself can then be easily obtained by regarding the edges between fore- and background of the binarized image trough a gradient-based approach [12]. The main disadvantage of the gradient based edge extraction is the fact, that resulting edges are usually wider than one pixel, which would either yield a non-injective discrete function by using all edge pixels admitting more than one sheet pixel at each location. Therefore, the resulting edge-image is skeletonised to get structures of an equal width as one pixel. As the remaining image consists of several edge-structures with no information about which pixel belongs to one of the sheet, the lamella pixels are identified through a direction oriented graph-search from the user defined beginning of the lamella at the lower end of the nozzle. To turn a set of pixels belonging to the sheet into a discrete function, the orthogonal distance of the pixels to the regression line is sampled at equidistant steps along the regression line, leading to the further analysed spray angels. For every single setting 150 frames with a framerate of 12.5 Hz were taken and analysed.

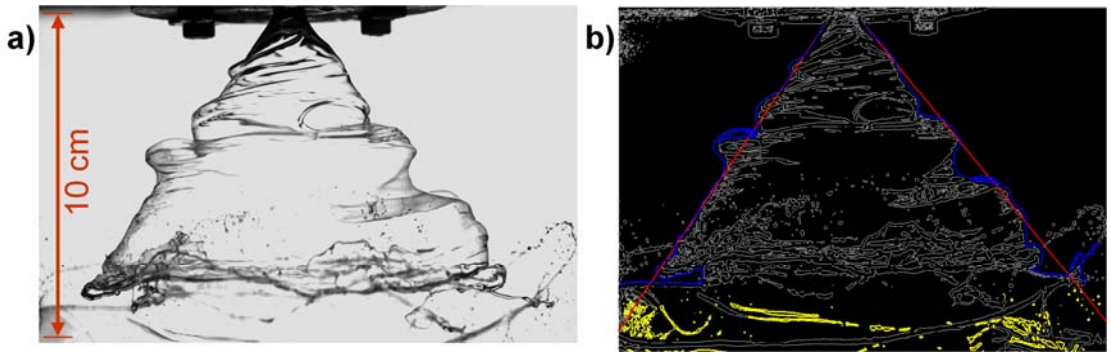

Figure 4 a) raw image of an spray cone at 0.3 MPa using water and D = 8 mm
b) binerized version of the raw image including the extracted spray angle

Signal extraction from the fiber sensor images is performed using the following image processing steps. At first, the given raw image is binarized to separate the sheet contour from the background. Therefore the horizontal image gradient is computed and adaptively thresholded to identify pixel representing the position of the sheet by means of sharp gray level transitions along the time axis. The vertical image gradient is ignored, since every single fiber produces intensity gradients along the fiber array that generally can not be distinguished from sheet-position induced gradients. The binary image is filtered by means of median and morphological filters to reduce noise effects and the resulting image shows a scattered version of the signal to extract. Additional filters may be inserted into the processing queue to enhance signal accuracy. In order to meet the demand of a fast, automatic and reproducible extraction, the second step consists of approximating the signal as indicated by scattered unconnected image regions by means of a dual active contour approach ("snake") [13]. Thereby, the amount of manual interaction is reduced significantly to accelerate the image evaluation process. A snake is an energy minimizing curve guided by external constraint forces and influenced by image forces that direct it towards desired image features, such as lines and edges. In the present approach, an additional force induces the two curves to move towards each other. Finally, the solution of partial differential equations associated with the active contour is computed by a finite difference scheme [14]. Following this procedure, all curves can be sampled and plotted as a discrete time/space-plot, which is the basis of further data evaluation.

Results and Discussion

During the course of this study, spray cone angles, sheet break-up lengths and various local sheet oscillation characteristics were determined for eight different nozzle geometries. The determined sheet oscillation characteristics include the dominating oscillation frequencies, as well as the local sheet velocities. Together with the flow capacity, the spray cone angle is essential for characterization of a nozzle. Atomization of various liquids at different atomization pressures lead to different spray angles. Since the impact of the liquid surface tension on the spray angle can be neglected, the pressure based Reynolds-number of the fluid, $Rep = (\rho \cdot \Delta p)^{0,5} \cdot D/\mu$, may be used

to characterize the nozzle behaviour for different operating conditions. In the present work an Re_p-range of $10^3 < Re_p < 2 \cdot 10^5$ has been examined using the photography method including different nozzle geometries, as shown in Fig. 5 (left). The plot indicates an increase of the spray cone angle at higher Re_p-numbers, also showing approximate saturation at very high Re_p-values. Here, the satiation is linked to the decreasing influence of the friction losses as depending on liquid viscosity. The highest possible value for spray angle is given by the nozzle geometry only and may be described by the swirl-ratio Δ. Considering the nozzle geometry listed in Table 1, it is shown that the resulting spray angles are directly linked to the swirl-ratios. An increase in swirl-ratio leads to an increase of the sheet velocity in tangential direction at the nozzle orifice resulting in higher spray angles. Here, the L/D-ratio 1 is leading to an slight decrease compared to L/D = 0 in the spray angle which is likely caused by energy losses based on turbulence effects, as the liquid passes alongside a corner at the transition from the conical part to the orifice. However, the plot in Fig. 5 (left) indicates also that for sharp edged orifices, i.e. L/D=0, the orifice diameter has almost no influence on the resulting spray angle, as long as the swirl chamber diameter D_K is kept equal. In this context, the inlet diameter D_E seems to have no significant influence on the spray angle. However, at low Re_p-numbers, $Re_p < 1000$, the liquid sheet forms a tulip and finally collapses.

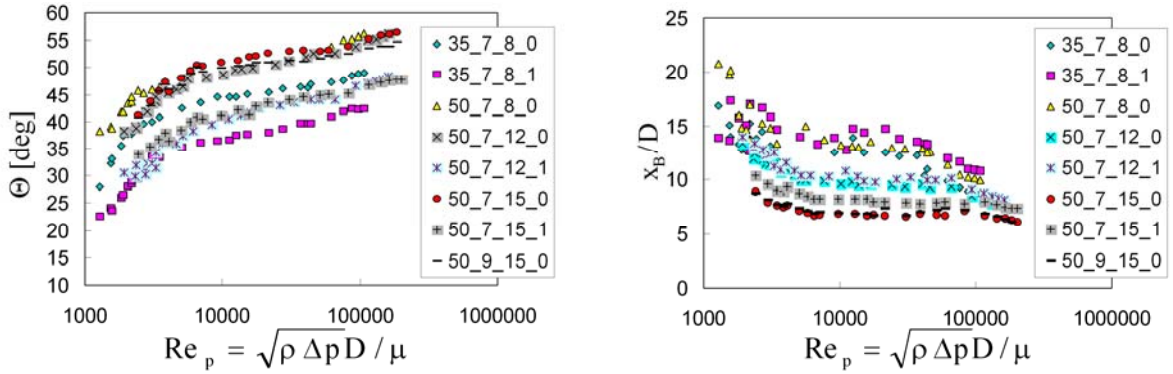

Figure 5 left: spray cone angle, right: dimensionless break-up length depending on Re_p and nozzle geometry (D_K_D_E_D_L/D [mm]), Δp = 0.03 MPa

Furthermore, the sheet signal continuity has been determined for different nozzle geometries. As the sheet propagates, it may contain some random holes, which become bigger due to rim contraction. Even with a fully continuous sheet without holes, the exact location of the sheet break-up is fluctuating over time. Because of these effects, the sheet break-up length x_B examined using the photography method, as shown in Fig. 4, may scatter when different images are compared. By average determination of multiple images, up to 300 per single setting, the data spread can be minimized, leading to the chart shown in Fig. 5. The spread of data lies within the size range of the symbols. The plot indicates a reverse trend to the spray angles determined, i.e. when the spray angle is increasing, the sheet tend to break-up earlier. Nozzles, which produce wider spray angles, show shorter break-up lengths. The middle of the examined Re_p-range shows some break-up length independency from the Re_p-number, although an increase in Re_p-number means also an increase in We-number, $We = \rho \cdot v_{eff}^2 \cdot D/\gamma$. Despite of the fact higher Weber numbers means a stronger gas/liquid-interaction and suggests shorter break-up lengths. At higher Re_p-numbers, $Re_p > 10^4$, the transition into the turbulent break-up regime is taking place, changing the shape of the sheet to a more rough form. During the data analysis, it was observed that the exact detection of the break-up location is much more difficult, when turbulence effects are present, which may have caused the independency from the Re_p-number. These observations indicate the limits of photographical methods for break-up localization. For this purpose, an alternative measuring system has to be included in the experimental characterization.

The sheet oscillation signal recorded with the fiber sensor shown in Fig. 3 may exhibit signal discontinuities, which represent the local sheet break-up course. By defining an upper limit for the signal continuity, from which on the sheet is treated as broken, the location of sheet break-up may be detected more accurately than by using the photographical method. The signal continuity for different nozzles, but one single pressure as an example, is shown in Fig. 6 for two liquid viscosities. The plot for a liquid viscosity of 1 mPas (water) shows, that the decrease of signal continuity along the main flow direction of the sheet is almost constant. Comparing the results with those obtained using the photography method as shown in Fig. 5 (right), it becomes apparent, that the ranking of the nozzle geometries is nearly the same. Nozzles with high swirl-ratios Δ lead to smaller signal continuities and thus to shorter break-up lengths. The break-up lengths obtained with photos seem to correspondent with a signal continuity of less than 0.4 (40 %), when the trends are extended to higher distances from the orifice. For higher liquid viscosities, as shown in Figure 6 (right), the drop in signal continuity is smaller, while the nozzle ranking is almost the same. Because of the higher spreading of data for x/D < 3, the range very close to the noz-

zle seem to be hardly detectable when higher viscous liquids are atomized. The signal continuity at close range to the nozzle is expected to be near 1 (100 %).

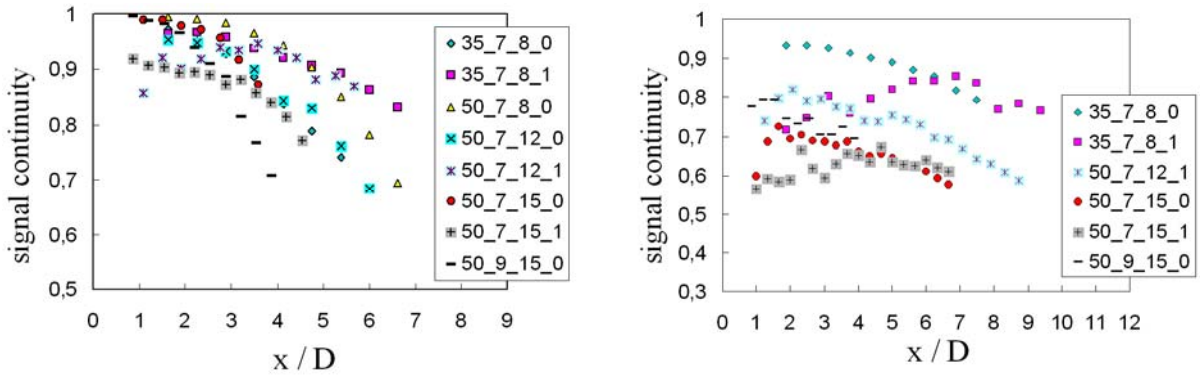

Figure 6 local sheet signal continuity, left: μ = 1 mPas, right: μ = 43.8 mPas, nozzle geometry (D_K_D_E_D_L/D [mm]), Δp = 0.03 MPa

Using a dual fiber-sensor setup, as described in [8], the local sheet velocities were measured. The results were plotted in Fig. 7 for low viscous (Fig. 7 left) and the high viscous case (Fig. 7 right), where the effective sheet velocity is related to the potential velocity calculated with the Bernoulli equation and the atomization pressure, leading to the velocity coefficient $\varphi = v_{eff}/_{pot}$. The chart shows that there is a significant drop in dimensionless velocity along the main moving path of the sheet. Thus, the local We-number is also depending on the distance from the nozzle orifice and is smaller as in the case, where the sheet velocity is assumed to be constant [1]. For a more accurate description of the drop formation process, a new model should be developed, which considers the sheet velocity decrease. For higher viscosities, as shown in Fig. 7 (right), the assumption of a constant sheet velocity may apply to the measured sheet behaviour, because the sheet velocity is nearly independent of the nozzle distance. The overall velocity-coefficient φ reaches smaller values compared to the case when low viscous liquids are atomized and friction losses increase. Here, a closer look to the sheet texture is necessary to describe this behaviour. The turbulences at low viscous liquids lead to a more textured sheet surface, which may be described as an increased surface roughness, leading to a more intensive momentum exchange with the ambient air causing the drop in velocity. Further investigations on this matter have to be made to quantify the momentum exchange. The ranking of the applied nozzle geometries is almost the same when compared to the spray angles in Fig. 5. Nozzles with a high swirl-ratio lead to higher sheet velocities.

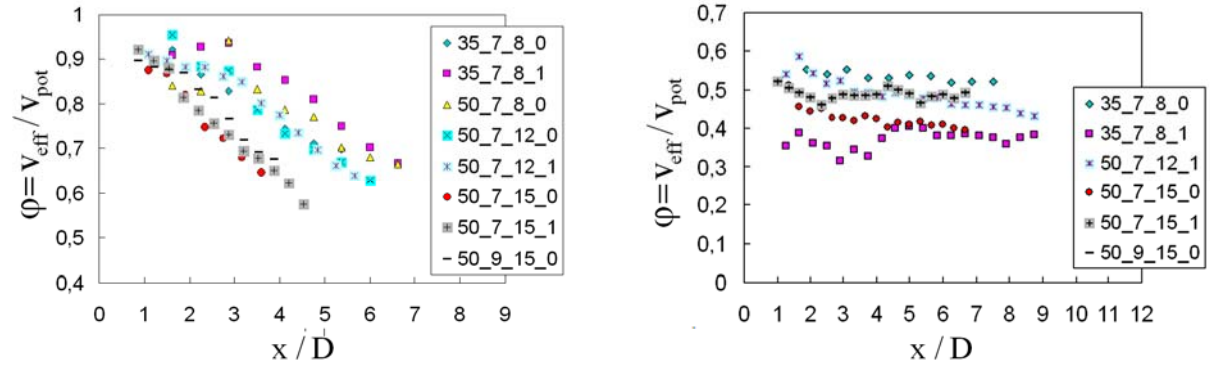

Figure 7 local sheet velocity number, left: μ = 1 mPas, right: μ = 43.8 mPas, nozzle geometry (D_K_D_E_D_L/D [mm]), Δp = 0.03 MPa

In addition, the stretching of the sheet due to the growth of oscillation amplitudes along the trajectories has been considered. Sheet stretching leads to reduced thickness, which is found to be neglected in several drop formation models in literature [1][2][3], although may be of importance for the drop size prediction. The experimental determination of this value is difficult, due to the small dimensions and the high sheet velocities. In general, the local sheet thickness may be measured using the laser-induced fluorescence (LIF) method, as shown in [15] for radialy spreading sheets. However, it is also possible to obtain the local sheet thickness indirectly by considering the mass flow conservation, the spray cone angle and the sheet stretching factor. The sheet stretching factor S is defined as the total curve length of the recorded sheet oscillation signal shown in Fig. 3 compared to the linear displacement within the same time increment. The higher the oscillation amplitude of the sheet, the

larger is the stretching factor. Thus, the stretching factor may be used to quantify the growth of amplitudes along the moving path of the sheets. As an example, the results of the measured streching factor for various nozzles are presented in Fig. 8. The plots indicate that larger nozzle diameters lead to higher stretching factors, while the influence of the L/D-ratio is found to be negligible for low viscous fluids, but very important at higher viscosities. In general, higher sheet velocities do not mean higher stretching ratios, although the local We-numbers are higher. The mechanism responsible for the growth of amplitudes is probably strongly depending on the viscosity or Reynolds number. At smooth sheets, as example when high viscous liquids are atomized, the stretching ratio is twice as large as for rough, i.e. low viscous sheets.

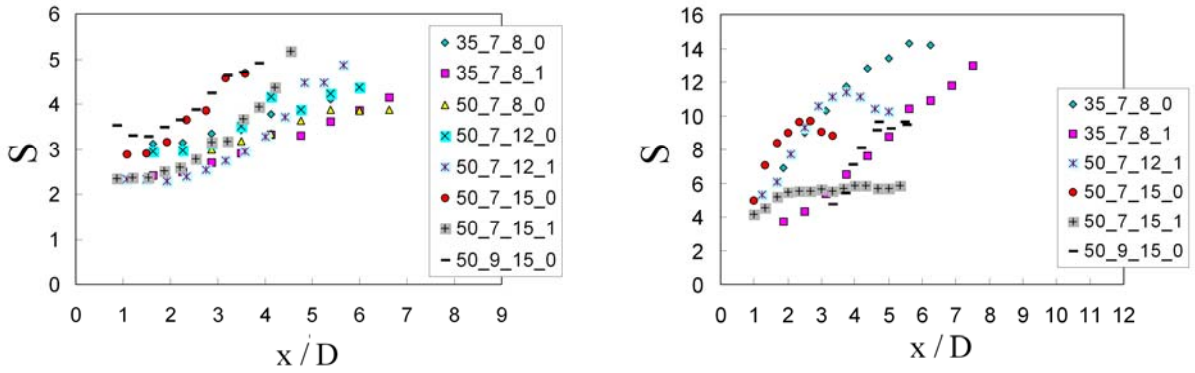

Figure 8 local signal stretching ratio, left: μ = 1 mPas, right: μ = 43.8 mPas, nozzle geometry (D_K_D_E_D_L/D [mm]), Δp = 0.03 MPa

Further physical values probably needed for the prediction of drop sizes is the dominating frequency found on the liquid sheet. The diameter of the emerging cylindrical shaped ligaments during the drop formation process is found to be directly linked to the sheet oscillation frequencies or the corresponding wavelengths [2][3]. However, experimental data of those frequencies are rarely found in literature. The major benefit of the fiber-sensor used in this work, is its ability to detect those frequencies in high spatial and temporal resolution. Fig. 9 represents results of the frequency measurements, where a dimensionless frequency, i.e. the local Strouhal-number St is plotted versus the dimensionless nozzle distance. Here, the inserted frequency is the dominating frequency found in the Fourier-spectra of the recorded signal. While the low viscous sheet, as shown in Fig. 9 (left), shows almost one dominating Strouhal-number for all distances, the high viscous liquid, as shown in Fig. 9 (right), shows a strong decrease. The nozzle ranking complies with the ranking found analyzing the spay angles, which were measured with a completely different measuring method. The decrease for high viscous liquids is probably caused by the elimination of higher frequency bands due to the stretching of the sheets, as a consequence of the viscosity. In the future, half-empirical correlations will be presented, allowing for a prediction of spray angles and dimensionless velocities for a wide range of nozzle geometries and operating conditions. Furthermore, the momentum exchange with the gas will be theoretically analyzed, which is the main cause of the velocity loss of the moving liquid sheet.

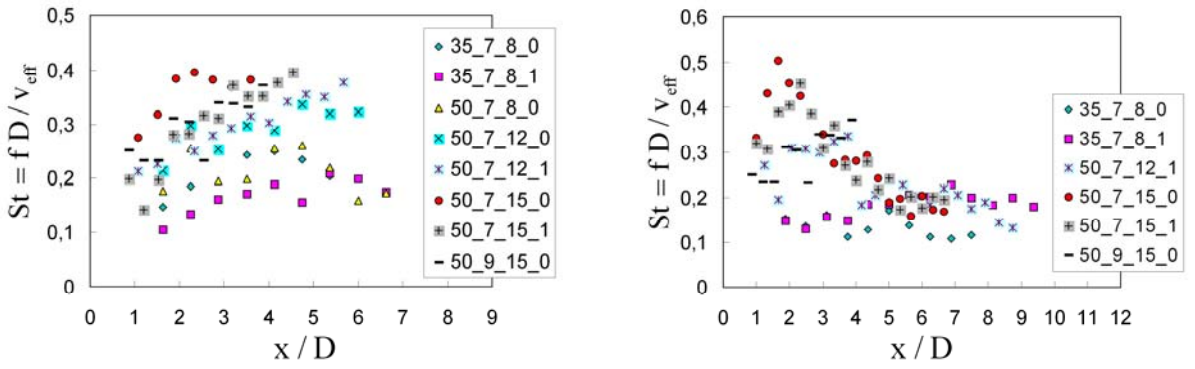

Figure 9 local sheet Strouhal-number, left: μ = 1 mPas, right: μ = 43.8 mPas, nozzle geometry (D_K_D_E_D_L/D [mm]), Δp = 0.03 MPa

Conclusions

The combination of a photographical method with a fiber-sensor has the benefit of an almost complete set of measured characteristics of oscillating liquid sheets. The investigations has shown connections between sheet oscillation frequencies and the growth of aerodynamic waves, as well as between the spray angles and the break-up lengths. Within the range examined, the frequency analysis of the sheet oscillation shows dominating oscillation frequencies at all flow conditions, which were found to be directly linked to the spray angles and sheet velocities. With growing distance to the nozzle orifice, the dominating frequency remains constant. The decrease in sheet thickness due to its spread along divergent streamlines, as well as caused by the growth of wave amplitudes can also be adressed with this method.

Acknowledgment

The authors want to express their gratitude to the German research foundation „Deutsche Forschungsgemeinschaft (DFG)“ for their financial support of the project.

Nomenclature

Symbol	quantity	SI Unit
A_E	nozzle inlet cross section	m²
D	nozzle orifice diameter	m
D_K	swirl chamber diameter	m
D_E	nozzle inlet diameter	m
f	oscillation frequency	1/s
L	length of the nozzle outlet	m
v_{eff}	local effective sheet velocity (absolute value)	m/s
v_{pot}	potential sheet velocity (absolute value)	m/s
r_A	nozzle orifice radius	m
r_E	radial distance of the nozzle inlet	m
S	sheet stretching ratio	-
x	sheet running length	m
x_B	sheet break-up length	m
Δp	pressure gradient	Pa
α	swirl chamber cone angle	deg
μ	dynamic liquid viscosity	kg/(m·s)
ρ	liquid density	kg/m³
γ	surface tension	kg/s²
Δ	swirl-ratio	-
Θ	spray cone angle	deg
$\varphi = v_{eff} / v_{pot}$	dimensionless sheet velocity	-
$Re_p = (\rho \Delta p)^{0,5} D / \mu$	pressure based Reynolds number	-
$We = (\rho v_{eff}^2 D) / \gamma$	Weber-number	-
$St = (f D) / v_{eff}^2$	Strouhal-number	-

References

[1] S. B. Squire, “Investigation of the Instability of a Moving Liquid Film”, *Brit. J. Appl. Phys.*, 4:1967- 1969 (1953)

[2] N. Dombrowski and W. R. Johns, “The Aerodynamic Instability and Disintegration of Viscous Liquid Sheets”, *Chem. Eng. Sci.*, 18: 203-214 (1963)

[3] Senecal at all, Modeling High-Speed Viscous Liquid Sheet Atomizationm, *Int. J. Multipase Flow*, 25: 1073-1097 (1999)

[4] C. Mehring and W.A. Sirignano, “Capillary Stability Of Modulated Swirling Liquid Sheets”, *Atomization and Sprays*, 14: 397-436 (2005)

[5] T.J. Tharakan, K. Ramamurthi, "Growth of Longitudinal Waves in Plane Liquid Sheets Having Lateral Waves Modes When Exposed to Two Gas Streams of Unequal Velocities", *Atomization and Sprays*, 15: 181-200 (2005)

[6] E. Musemic, A. Rojek, M. Gasper, F. Weichert, H. Müller and P.Walzel, "Experimental Analysis and 3D-Visualization of Oscillating Hollow-Conical Liquid Sheets in Quiescent Air", *ICLASS 2008*, Vail, Colorado, USA, 26-30 Jul. 2009, A174

[7] P. Broll and P. Walzel, "PIV Measurements in Pressure Swirl Atomizers", *ILASS-Europe 2001*, Zurich, 2-6 Sep., 2001

[8] E. Musemic, P. Walzel, M. Gasper and F. Weichert, "Analysis of Multiphase Flow during the Process of Sheet Disintegration at Hollow Cone Nozzles using Multiple One-Dimensional Fibre-Sensors", *ILASS-Europe 2008*, Como, Italy, 8-10 Sep. 2008, A075

[9] F. Landwehr, H. Wiggers, and P. Walzel, "A New Technique for Multi-Phase Spray Analysis at High Loads", *ILASS-Europe 2001*, Zurich, 2-6 Sep., 2001

[10] F. Landwehr, F., Feggeler, D., Walzel, P., Weichert, F., Schröter, S. and Müller, H., "A Fibre Sensor Based Frequency Analysis of Surface Waves at Hollow Cone Nozzles", *Experiments in Fluids*, 40:523-532 (2005)

[11] L. Huang and M. J. Wang, "Image thresholding by minimizing the measures of fuzziness", *Pattern Recognition*, 28(1):41-55 (1995)

[12] R. C. Gonzalles, R. E. Woods and S. L. Eddins, "Digital Image Processing Using Matlab", Pearson Prentice Hall, pp. 5-11

[13] M. Kass, A. Witkin and D. Terzopoulos, "Snakes: Active Contour Models", *Int. J. of Computer Vision*, 1: 321-331 (1988)

[14] W. Press, S. Teukolsky, W. Vetterling and B. Flannery, "Numerical Recipes in C. 2nd edition", *Cambridge University Press*, 1992

[15] T.Wakimoto, T. Azuma, "Instability of Radial Liquid Sheet Flow", JSME Int. J., Series B., 47(1):9-19 (2004)